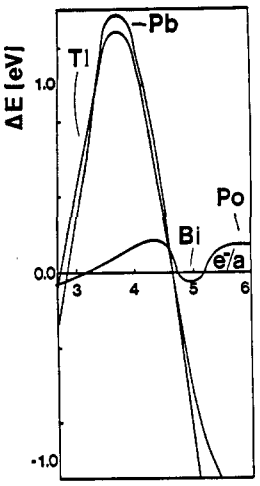

Figure 5. The difference in energy between the Tl, Pb, bi, and Po structures as a function of electron count. Parameters used were $H_{ii}(4s) = -30.0$ eV, $\zeta(4s) = 3.5$; $H_{ii}(4p) = -9.0$ eV, $\zeta(4p) = 1.85$. Differences in energy between a given structure and the Bi structure are plotted. See Figures 2 and 3 for figure conventions and calculational details.

One general trend is clear. In the case of two or three types of electrons (s, p, or d) the energetically lowest band exerts relatively little stereochemical control. For example, were Pettifor to have contracted the d orbitals in his calculation on the later transition elements, he would have found that Cu should indeed be in the fcc structure type as is known to be experimentally correct. Similarly, we have contracted the s orbitals more than standard literature values would lead us to believe in the case of the heavier main group atoms.[13]

This difference can be traced to the use of Hückel and not extended Hückel theory. In the Hückel theory of extended solids the most bonding molecular orbital is calculated to be at an unrealistically low energy. As we wish to place the s band near the bottom of the p band we must therefore place the H_{ii} Coulombic value of the s orbitals at a rather low energy. This choice of a low energy for the H_{ii} value of the s orbital in turn has an effect on the overall size of the s orbital. This is so as we use the Wolfsberg-Helmholz approximation for the off-diagonal H_{ij} elements. In this approximation an increase in the magnitude of H_{ii} directly increases the value of H_{ij} (see preceding section). As we have used unrealistically low H_{ii} values to compensate for the deficiencies of Hückel theory, we must therefore rely on small overlap integrals, S_{ij}, so that the overall magnitude of the off-diagonal elements H_{ij} is correct. In order to have small S_{ij} values we use overly contracted Slater exponents, ζ, in describing our Slater-type orbitals.

In our work we have used an average set of atomic parameters to resolve the trends that occur within a given row of the periodic table. One drawback of this method is that we are unable to introduce element-specific features into our calculations. However, it has been previously shown that several element-specific distortions are found in structures such as Zn, Cd, Ga, and In. As such distortions do not greatly change the ring structures of the systems it is generally not possible for our generic elemental model to resolve these distortions. For example, we were unable to explain why In has distorted from the fcc structure.

Finally, it should be noted that the energetic results of a Hückel calculation are unable to explain the stability of the P_4 or As_4 tetrahedron. See ref 5 for a discussion of this problem.

Acknowledgment. I would like to thank the Petroleum Research Fund, administered by the American Chemical Society, and the Rackham Graduate School for partial support of this research. The band program used in our calculations is a modified version of the program written at Cornell University by Roald Hoffmann, M.-H. Whangbo, T. Hughbanks, S. Wijeyesekera, M. Kertesz, C. N. Wilker, and C. Zheng. I also thank Dr. G. Miller for this irreducible wedge k-space programs.

Theoretical Study on the Electronic Spectra of Model Compound II Complexes of Peroxidases

Ping Du,*,† Frank U. Axe,† Gilda H. Loew,† Silvio Canuto,‡,§ and Michael C. Zerner‡

Contribution from the Molecular Research Institute, 845 Page Mill Road, Palo Alto, California 94304, and Department of Chemistry, University of Florida, Gainesville, Florida 32611. *Received March 29, 1991*

Abstract: A quantum chemical study of the electronic structure and spectra of four compound II iron porphyrin complexes with varying axial ligands, Cl^- (Hemin), pyridine, imidazole, and imidazolate (model peroxidase), has been carried out using the INDO/S method. These calculations confirm the nature of the triplet ground state as one in which the two unpaired electrons occupy the Fe-O π^* orbitals that are primarily Fe(IV) $3d_{xz}$ and $3d_{yz}$. About 20% of the unpaired spin density is calculated to be on the oxygen atom, in agreement with the experimental estimate of about 25%. The calculated spectra show that charge-transfer (CT) transitions exist for all compound II complexes. The excitation energies for these CT transitions are estimated to be between the Q and B (Soret) bands and to have moderate oscillator strengths. Although a description of the CT excited state for each of the model systems is complex, an electron transition from the porphyrin π orbitals to the Fe-O π^* orbitals is a common component. For Hemin-II, an additional component of the CT transition wave function is an excitation from the Cl $3p_z$ orbital to the porphyrin $4e_g$ orbitals. For the pyridine and imidazole complexes, there is a mixing in the CT of an excitation from the porphyrin π to a ligand π^* orbital. For the complex with an imidazolate ligand, mixing of porphyrin $\pi \rightarrow \pi^*$ excitations was found. The fact that the model compound II complexes with both a neutral imidazole and a deprotonated imidazolate ligand have CT transitions between Q and B does not allow us to use spectral properties to predict the actual form of this intermediate in the reaction mechanism of protein.

Introduction

Iron-oxo compounds are proposed to participate in the biochemical cycles of several different kinds of heme enzymes to perform essential oxidations in various biochemical pathways.[1-5] For instance, cytochrome c peroxidase (CCP), horseradish per-

† Molecular Research Institute.
‡ University of Florida.
§ Permanent address: Department de Fysica, Universidade de Pernambuco, Recife, Brazil.

(1) Poulos, T. L. *Adv. Inorg. Biochem.* **1988**, *7*, 1.
(2) Poulos, T. L.; Finzel, B. C. In *Peptide and Protein Reviews*; Hearn, M. T. W., Ed.; Marcel Dekker: New York, 1984; Vol. 4, p 115.
(3) Ortiz de Montellano, P. R. *Acc. Chem. Res.* **1987**, *20*, 289.

0002-7863/91/1513-8614$02.50/0

oxidase (HRP), and catalase (CAT), when activated by peroxides and peracids, form an iron–oxo compound I intermediate (eq 1a).

$$\text{enz} + \text{ROOH} \rightarrow \text{compound I} + \text{ROH} \quad (1a)$$

$$\text{compound I} + \text{AH}_2 \rightarrow \text{compound II} + \text{AH}^\bullet \quad (1b)$$

$$\text{compound II} + \text{AH}_2 \rightarrow \text{enz} + \text{AH}^\bullet \quad (1c)$$

$$\text{AH}^\bullet + \text{AH}^\bullet \rightarrow \text{nonradical products} \quad (1d)$$

In general, peroxidase substrate oxidation occurs in two steps involving a second, once-reduced enzyme intermediate, compound II (eq 1b) which is reduced back to the original ferric resting state. The free radicals formed in eqs 1b and 1c usually dimerize to give nonradical products (eq 1d). By contrast, in catalase, compound I performs simultaneous two-electron reductions of its peroxide substrate. In CCP, compound I, which is believed to be formed initially, rapidly transfers one of its oxidizing equivalents from the heme unit to a nearby residue, now thought to be Trp 191,[6] forming a compound II like species, called compound ES.

Compound I is also believed to be formed in the reactions of the mixed function oxygenases, the cytochrome P450s. Instead of reacting with a peroxide, P450 is activated in a more complex cycle involving two sequential electron reductions with addition of molecular oxygen in an intervening step.[3,5] The oxidations catalyzed by the putative iron–oxo species in P450 are different from that of CCP, HRP, and CAT. In P450, the compound I species transfers a single atom of oxygen directly to a variety of substrates. While CAT and HRP compound I complexes are stable enough to have been studied by a variety of spectroscopic techniques,[1-5] the putative P450–compound I has not been characterized, presumably because it has an extremely short lifetime, and the evidence for it is hence indirect.

The importance of iron–oxo compounds in biological systems as well as their relevance to catalysis has stimulated the development of model heme complexes of compounds I and II in order to probe the chemistry of these reaction intermediates without the modulation of the protein environment.[7] These model compounds are found in general to mimic to some extent the catalytic behavior found at the active site of cytochrome P450s. Similarities in chemistry and electronic absorption spectra[7] of the model systems to the intact heme proteins suggest that the basic electronic structure of the heme unit in both systems is the same. However, the protein environment of the heme unit in various families of metabolizing heme proteins further modulates the differences in the manner in which they oxidize their substrates.

The electronic structure of compounds I and II complexes of intact heme proteins, particularly HRP, as well as a number of model heme complexes has been a subject of extensive theoretical and experimental investigations. Model compounds I and II complexes have been treated by a number of theoretical methods, including charge iterative extended Huckel,[8,9] UHF INDO,[10] and UHF[11-13] and RHF[14,15] ab initio calculations. In these latter studies, a model compound I and compound II with pyridine ligand has been elucidated by Yamamoto et al. with a CASSCF method.[14] These combined results all indicate that the ground state of the compound I species is a quartet porphyrin π cation radical and that compound II is a triplet state in which the added electron reduces the porphyrin ring, leaving the environment around the iron and the active oxygen and the nature of the Fe–O bond intact. In both compounds I and II, two unpaired electrons are delocalized in a molecular orbital confined primarily to the Fe $3d_\pi$ and O $2p_\pi$ atomic orbitals and the iron is in a formal Fe(IV) state. This observation is responsible for the very similar Fe nuclear properties for compounds I and II.[14,15]

The experimental techniques used to characterize the ground and low-lying excited states of compounds I and II species include magnetic susceptibility,[16,17] Mossbauer resonance,[18,19] ESR[20] and ENDOR[21] spectroscopy, X-ray crystallography,[22,23] and EXAFS.[24,25] For example, quadrupole splitting from Mossbauer resonance experiments[18,19] on heme proteins and compounds I and II model complexes yields very similar values of ~15 mm/s. ESR[20] and ENDOR[21] data are all consistent with the Fe(IV) configuration of iron, and the ENDOR experiments provide a quantitative measurement of the oxygen atom spin density. Structural data on these transient species is limited.[23-25] However, it is relatively well established from EXAFS[24,25] and X-ray crystallography[23] that the iron–oxo bond lengths are all about 1.7 Å.

The electronic absorption spectra of compound I and compound II species have also been investigated[17,26-30] and exhibit interesting common transitions in addition to the normal heme Q and B (Soret) porphyrin π to π^* transitions. Specifically, the spectra of CCP-II,[28] and Hemin-II,[29] and a model compound II with a pyridine ligand[17] show common extra absorptions in the frequency range between Q and B. The purpose of this paper is to assign the optical spectra of compound II complexes and particularly to account for these extra features. To this end, we have performed ROHF-SCF and CI calculations, using the semiempirical intermediate neglect of differential overlap method parameterized for spectroscopy (INDO/S) on the four model compound II complexes. The effect of deprotonation of the imidazole ligand on the electronic absorption spectra has been studied by comparing the calculated spectra of the model complexes with imidazole and imidazolate ligands. The calculated extra features of these compound II complexes relative to normal heme absorptions are discussed. In addition, in these studies we have verified the description of the ground electronic state. The simpler electronic structure and lower spin multiplicity of compound II provide the basis for future calculations of compound I structure and spectra.

Methods

All calculations of the model compound II complexes were carried out using a spin-restricted open-shell INDO method, which is described in detail elsewhere[31-37] The electronic spectra were calculated using a

(4) Dawson, J. H.; Elbe, K. S. *Adv. Inorg. Bioinorg. Mech.* **1986**, *4*, 1.
(5) Ortiz de Montellano, P. R. In *Cytochrome P-450*; Ortiz de Montellano, P., Ed.; Plenum Press: New York, 1986; p 217.
(6) Erman, J. E.; Vitello, L. B.; Mauro, J. M.; Kraut, J. *Biochemistry* **1989**, *28*, 7992.
(7) McMurry, T. J.; Groves, J. T. In *Cytochrome P-450*; Ortiz de Montellano, P., Ed.; Plenum Press: New York, 1986; p 1.
(8) Loew, G. H.; Kert, C. J.; Hjelmeland, L. M.; Kirchner, R. F. *J. Am. Chem. Soc.* **1977**, *99*, 3534.
(9) Hanson, L. K.; Chang, C. K.; Davis, M. S.; Fajer, J. *J. Am. Chem. Soc.* **1981**, *103*, 663.
(10) Loew, G. H.; Herman, Z. S. *J. Am. Chem. Soc.* **1980**, *102*, 6173.
(11) Strich, A.; Veillard, A. *Theor. Chim. Acta* **1981**, *60*, 379.
(12) Strich, A.; Veillard, A. *Nouv. J. Chim.* **1983**, *7*, 347.
(13) Yamaguchi, K.; Takahara, Y.; Fueno, T. In *Applied Quantum Chemistry*; Smith, V. H., Jr., Schaefer, H. F., Morokuma, K., Eds.; Reidel: Dordrecht, 1986; p 155.
(14) Yamamoto, S.; Teraoka, J.; Kashiwagi, H. *J. Chem. Phys.* **1988**, *88*, 303.
(15) Yamamoto, S.; Kashiwagi, H. *Chem. Phys. Lett.* **1988**, *145*, 111.
(16) Theorell, J.; Ehrenberg, A. *Arch. Biochem. Biophys.* **1952**, *41*, 442.
(17) Chin, D.; Balch, A. L.; La Mar, G. N. *J. Am. Chem. Soc.* **1980**, *102*, 1446.
(18) Moss, T. G.; Ehrenberg, A.; Bearden, A. J. *Biochemistry* **1969**, *8*, 4159.
(19) Harami, T.; Maeda, Y.; Morita, Y.; Trautwein, A.; Gonser, U. *J. Chem. Phys.* **1977**, *67*, 1164.
(20) Schulz, C. E.; Devaney, P. W.; Winkler, H.; DeBrunner, P. G.; Doan, N.; Chiang, R.; Rutter, R.; Harger, L. P. *FEBS Lett.* **1979**, *103*, 102.
(21) Roberts, R.; Hoffman, B. M.; Rutter, R.; Hager, L. P. *J. Am. Chem. Soc.* **1981**, *103*, 7654.
(22) Piciulo, P. L.; Ruppecht, G.; Scheidt, W. R. *J. Am. Chem. Soc.* **1974**, *96*, 5293.
(23) Schapperacher, M.; Weiss, R. *J. Am. Chem. Soc.* **1985**, *107*, 3736.
(24) Chance, B.; Powers, L.; Ching, Y.; Poulos, T.; Schonbaum, G. R.; Yamazaki, I.; Paul, K. G. *Arch. Biochem. Biophys.* **1984**, *235*, 596.
(25) Penner-Hahn, J. E.; Eble, K. S.; McMurry, T. J.; Renner, M.; Balch, A. L.; Groves, J. T.; Dawson, J. H.; Hodgson, K. O. *J. Am. Chem. Soc.* **1986**, *108*, 7819.
(26) Dunford, H. B. *Adv. Inorg. Biochem.* **1982**, *4*, 41.
(27) Mansuy, D.; Lange, M.; Chottard, J. C. *J. Am. Chem. Soc.* **1979**, *101*, 6437.
(28) Yonetani, T.; Anni, H. *J. Biol. Chem.* **1987**, *262*, 9547.
(29) Groves, J. T.; Watanabe, Y. *J. Am. Chem. Soc.* **1986**, *108*, 507.
(30) Gold, A.; Jayaraj, K.; Doppelt, P.; Weiss, R.; Chottard, G.; Bill, E.; Ding, X.; Trautwein, A. X. *J. Am. Chem. Soc.* **1988**, *110*, 5756.
(31) Ridley, J. E.; Zerner, M. C. *Theor. Chim. Acta* **1973**, *32*, 111.
(32) Ridley, J. E.; Zerner, M. C. *Theor. Chim. Acta* **1976**, *43*, 223.

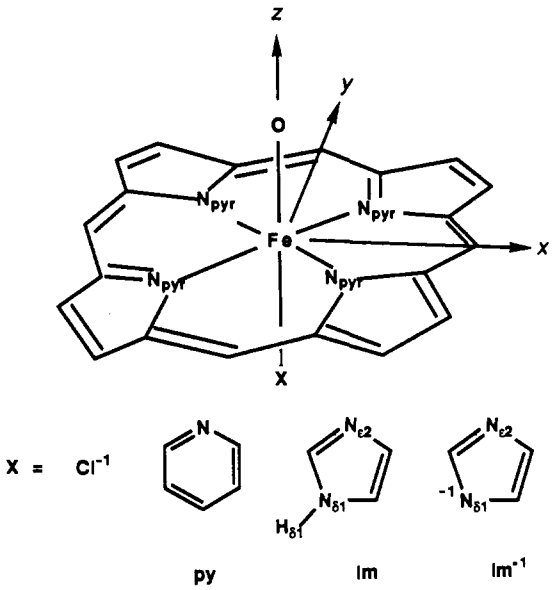

Figure 1. Model compound II structures and the coordination system.

singles only CI (CI-S) within the INDO semiempirical approximations, a model which has been parametrized for spectroscopy. The configurations were generated using the Rumer diagram technique.[38] Oscillator strengths were also calculated for each excited state relative to the ground state. A previous application of the same method, using 15 model heme complexes, has shown its reliability in predicting the relative energies and the correct assignment of the ground spin states of ferric heme complexes.[39] In addition, it has also been successfully used for the detailed calculation of the spectra of a number of radical heme species.[36,37,40]

The geometry of the porphyrin macrocycle for the model complexes was based on the X-ray crystal structure of iron tetraphenylporphyrin.[22] The porphyrin crystal structure was modified to porphine and idealized to D_{4h} symmetry. Although the actual complexes have lower symmetry, D_{4h} symmetry labels are used for the MOs and states calculated as they are traditionally in porphyrin chemistry. The orbitals that are primarily confined on the Cl–Fe–O fragment of the molecule are labeled as σ_1, π_1, etc. (see later discussions). The ligand π orbitals are labeled with an abbreviation of the ligand, e.g., py π_3 for the third π orbital of pyridine. The iron atom was placed in the porphyrin plane with the Fe–$N_{porphyrin}$ distance set to 2.01 Å. The Fe–O distance in all model systems was assumed to be 1.70 Å. The AM1[41] optimized geometries of pyridine and imidazole were used. The Fe–pyridine distance was set at 2.03 Å[14] and the Fe–imidazole distance at 2.02 Å.[2] The Fe–Cl distance of the Hemin compound II model complex was set at 2.20 Å.[42] The orientation of the complexes was such that the pyrrole nitrogens of the porphyrin macrocycle bisect the x and y axes and the Fe binding atom of the axial ligands lies on the z axis. The pyridine and imidazole ligands are in the xz plane (Figure 1).

Results and Discussion

I. Hemin-II Model Complex. C_{4v} symmetry was imposed on the ground state of the model Hemin-II complex. Since there is a single electron in each Cl–Fe–O π^* MO, the state symmetry is $^3A_2$. Table I summarizes the Mulliken populations calculated with the ROHF-SCF wave function for the ground state. Assuming that the INDO basis is related to a valence Slater basis

Table I. Ground-State Properties of Model Compound II Complexes

	Cl^-	pyridine	imidazole	imidazolate(1−)
		Mulliken Population		
Fe $3d_{z^2}$	0.98	0.99	0.96	0.95
$3d_{z^2-y^2}$	2.00	2.00	2.00	2.00
$3d_{xy}$	0.53	0.55	0.55	0.52
$3d_{xz}$	1.19	1.20	1.22	1.21
$3x_{yz}$	1.19	1.20	1.22	1.21
O $2p_x$	1.80	1.79	1.77	1.77
$2p_y$	1.80	1.79	1.77	1.78
$2p_z$	1.24	1.17	1.23	1.27
		Spin Population		
Fe $3d_{xz}$	0.81	0.80	0.77	0.78
$3x_{yz}$	0.81	0.80	0.77	0.78
O $2p_x$	0.17	0.19	0.21[a]	0.20
$2p_y$	0.17	0.19	0.21	0.20
		Net Charge		
Fe	1.70	1.40	1.45	1.45
porphyrin	−0.83	−0.79	−0.72	−0.90
ligand	−1.01	0.16	0.15	−0.71
O	−0.86	−0.77	−0.78	−0.84
total	−1.00	0.00	0.00	−1.00
		Quadrupole Splittings		
ΔE_Q (mm/s)	1.41	1.48	1.52[b]	1.43
η	0.00	0.00	0.00[b]	0.00
		Anisotropic Hyperfine (KG)		
A_{xx}	273	268	260	263
A_{yy}	273	267	259	263
A_{zz}	57	55	54	54

[a] Experimental value 0.25, ref 21. [b] Experimental values 1.46 and 0.03, ref 18.

Table II. Cl–Fe–O π MO Coefficients of Model Compound II of Hemin

MO	Cl $3p_x$	Fe $3d_x$	O $2p_x$
$\pi_{3x}{}^{*a}$	0.08	0.90	−0.42
π_{2x}	−0.67	0.10	0.22
π_{1x}	0.32	−0.36	−0.57

[a] This MO and the symmetry equivalent $\pi_{3y}{}^*$ are singly occupied, yielding a ground state of $^3A_2$ symmetry.

Table III. Cl–Fe–O σ MO Coefficients of Model Compound II of Hemin

MO[a]	Cl $3p_z$	Fe $4p_z$	Fe $3d_{z^2}$	O $2p_z$
$\sigma_4{}^*$	−0.23	0.64	0.11	0.26
$\sigma_3{}^*$	−0.32	−0.30	0.67	0.50
σ_2	−0.65	0.16	0.00	−0.33
σ_1	−0.35	−0.01	−0.61	0.66

[a] σ_1 and σ_2 are doubly occupied; $\sigma_3{}^*$ and $\sigma_4{}^*$ are unoccupied.

through symmetric orthogonalization, the Cl–Fe–O π electron population on Fe (sum of $3d_{xz}$ and $3d_{yz}$) is about 2.4, and that on O (sum of $2p_x$ and $2p_y$) is 3.6. Although the spin density is mostly located on the Fe, there is an appreciable amount of delocalization to the oxygen atom. The sum of the spin densities on these two atoms accounts for almost all of the electron spin of the complex. Spin delocalizations to Cl and the porphyrin are very small and are not listed.

Table II shows the coefficients of the Cl–Fe–O π_x MOs. The bonding and nonbonding MOs, π_{1x} and π_{2x}, respectively, are doubly occupied, with π_{2x} localizing on Cl $2p_x$, which can be regarded as a lone pair of Cl^-. The antibonding MO $\pi_{3x}{}^*$ is mostly an out-of-phase combination of Fe $3d_{xz}$ and O $2p_x$. It has very little contribution from the Cl $2p_x$, consistent with the spin distributions listed in Table I. The Cl–Fe–O π_y orbitals, which are not shown in Table II, are equivalent to the π_x orbitals. Table III shows the Cl–Fe–O σ MO coefficients. The two bonding orbitals, σ_1 and σ_2, are occupied, and the two antibonding orbitals, $\sigma_3{}^*$ and $\sigma_4{}^*$, are unoccupied. Contributions of the Cl 2s and O 2s atomic orbitals to the σ MOs are small and are not included in the table.

(33) Bacon, A. D. Ph.D. Dissertation, Department of Chemistry, University of Guelph, Canada, 1976.
(34) Bacon, A. D.; Zerner, M. C. *Theor. Chim. Acta* **1979**, *53*, 21.
(35) Edwards, W. D.; Zerner, M. C. *Theor. Chim. Acta* **1987**, *72*, 347.
(36) Edwards, W. D.; Weiner, B.; Zerner, M. C. *J. Am. Chem. Soc.* **1986**, *108*, 2196.
(37) Edwards, W. D.; Weiner, B.; Zerner, M. C. *J. Phys. Chem.* **1988**, *92*, 6180.
(38) Zerner, M. C.; McKelvey, J.; Edwards, W. D. Unpublished work. See also: Pauncz, R. *Spin Eigenfunctions*; Plenum Press: New York, 1979.
(39) Axe, F. U.; Flowers, C.; Loew, G. H.; Waleh, A. *J. Am. Chem. Soc.* **1989**, *111*, 7333.
(40) Du, P.; Loew, G. H. *J. Phys. Chem.* **1991**, *95*, 6379.
(41) Dewar, M. J. S.; Zoebisch, E. G.; Healy, E. F.; Stewart, J. J. P. *J. Am. Chem. Soc.* **1985**, *107*, 3902.
(42) Koenig, D. F. *Acta Crystallogr.* **1965**, *18*, 663.

Table IV. INDO/S CI-S Calculated Excited States of Model Compound II of Hemin

	theory[a]					experiment[c]	
state	dominant configurations and coefficient squared[b]	ΔE, kK	$f \times 10^3$	polarization	label	ΔE, kK	$\epsilon \times 10^{-3}$, mM^{-1} cm^{-1}
1^3E	$(1a_{1u},4e_g)$ 0.54, $(3a_{2u}-\sigma_2,4e_g)$ 0.37	9.2	0		triptriplet		
2^3E	$(d_{x^2-y^2},\pi_3^*)$ 0.96	10.0	0		d–d		
3^3E	$(3a_{2u}-\sigma_2,4e_g)$ 0.56, $(1a_{1u},4e_g)$ 0.40	11.4	0		triptriplet		
4^3E	$(3a_{2u}-\sigma_2,4e_g)$ 0.49, $(1a_{1u},4e_g)$ 0.47	14.7	26	xy	Q	14.3	0.06
5^3E	$(1a_{1u},4e_g)$ 0.53, $(3a_{2u}-\sigma_2,4e_g)$ 0.38	16.7	2	xy			
6^3E	(π_3^*,d_{xy}) 0.81	17.4	8	xy	CT, d–d	17.0	0.08
7^3E	$(3a_{2u}-\sigma_2,4e_g)$ 0.53, $(1a_{1u},4e_g)$ 0.42	18.9	2	xy			
9^3E	$(\sigma_2+3a_{2u},4e_g)$ 0.27, $(3a_{2u}-\sigma_2,\pi_3^*)$ 0.20, $(1a_{1u},4e_g)$ 0.09	22.2	274	xy	CT1	19.6	0.18
10^3E	$(\sigma_2+3a_{2u},4e_g)$ 0.31, $(1a_{1u},4e_g)$ 0.14, $(2b_{2u},4e_g)$ 0.11, $(3a_{2u}-\sigma_2,4e_g)$ 0.11, $(3a_{2u}-\sigma_2,\pi_3^*)$ 0.11	23.4	614	xy	B′		
5^3A_2	$(3e_g-\pi_2,4e_g)$ 0.21, $(3a_{2u}-\sigma_2,\sigma_3^*)$ 0.16, $(\pi_2+3e_g,4e_g)$ 0.15	23.6	2	z			
11^3E	$(3a_{2u}-\sigma_2,\pi_3^*)$ 0.29, $(3a_{2u}-\sigma_2,4e_g)$ 0.22, $(1a_{1u},4e_g)$ 0.13, $(\sigma_2+3a_{2u},4e_g)$ 0.12, $(2b_{2u},4e_g)$ 0.04	25.3	922	xy	B	24.4	1.26
7^3A_2	$(3e_g-\pi_2,4e_g)$ 0.37, $(3a_{2u}-\sigma_2,\sigma_3^*)$ 0.12, $(2e_g,4e_g)$ 0.07	26.4	1	z			
8^3A_2	$(3a_{2u}-\sigma_2,\sigma_3^*)$ 0.48, $(\pi_3^*,4e_g)$ 0.11, $(\sigma_2+3a_{2u},\sigma_3^*)$ 0.10	27.9	18	z			
10^3A_2	$(3e_g-\pi_2,4e_g)$ 0.27, $(3a_{2u}-\sigma_2,2b_{1u})$ 0.11, $(\sigma_2+3a_{2u},2b_{1u})$ 0.08	28.2	2	z			
13^3E	$(1a_{1u},\pi_3^*)$ 0.73	29.3	2				
14^3E	$(\sigma_2+3a_{2u},4e_g)$ 0.34, $(2b_{2u},4e_g)$ 0.30	29.8	60				
16^3E	$(\pi_2+3a_{2u},\sigma_3^*)$ 0.25, $(\sigma_2+3a_{2u},4e_g)$ 0.21, (π_1+3e_g,σ_3^*) 0.15	31.7	735	xy	CT2		
17^3E	$(\pi_2+3a_{2u},\sigma_3^*)$ 0.26, $(\sigma_2+3a_{2u},4e_g)$ 0.15, (π_1+3e_g,σ_3^*) 0.14	32.2	856	xy			
20^3E	$(1a_{1u},5e_g)$ 0.17, (σ_1,σ_3^*) 0.16, (π_1+3e_g,σ_3^*) 0.13	34.9	1074	xy			
24^3E	$(3e_g-\pi_2,d_{xy})$ 0.54, (π_2+3e_g,d_{xy}) 0.37	37.2	304	xy			

[a] E(SCF) = −201.817 345 au. CI-S includes 27 MOs (number 51–77) of the ground-state $^3A_2$ calculated with ROHF-SCF. All low-lying states are listed. For the transitions between 16.0 and 30 kK only those with nonzero oscillator strengths are listed. Between 30 and 40 kK, only strong transitions are listed. [b] MO notations: $1a_{1u}$ etc. are for porphyrin π MOs, d_{xy} etc. are for Fe AOs, and σ_1, π_1, etc. are for Cl–Fe–O MOs. See Tables II and III for definitions. A combined notation, $3a_{2u}-\sigma$ for example, means a mixing between the two fragment orbitals. The first is always the larger component. [c] Reference 29.

The CI-S calculation for the absorption spectrum was performed with 27 active MOs, which include 9 bonding porphyrin π MOs, 6 Cl–Fe–O π and σ MOs, 7 porphyrin π^* MOs, 3 Cl–Fe–O π^* and σ^* MOs, and the Fe(IV) $3d_{x^2-y^2}$ and $3d_{xy}$. Figure 2 shows the energy diagram of these MOs, with those that are involved in the dominant configurations of the excited states being labeled. These labels show the most important mixings between some of these orbitals that reduce their symmetry from D_{4h} to C_{4v}. For example, $3a_{2u}-\sigma_2$ is an out-of-phase combination of porphyrin $3a_{2u}$ with Cl–Fe–O σ_2. In this notation, the first fragment orbital always has the larger weight.

The calculated transitions from the ground state, 1^3A_2, to the ^3E states of the model hemin-II are x,y polarized. The calculated excitation energies and oscillator strengths for these transitions are listed in Table IV. The dominant configurations and the corresponding coefficient squared of each excited state are shown in the table to help analyze the major type of excitations involved in the observed transitions. For comparison, identified experimental transitions from a model Hemin-II study[29] are also listed in the table. A plot of the calculated spectrum is shown in Figure 3a.

All states with excitation energies below Q are listed in Table IV. These are two "triptriplet" states, resulted from the spin exchange coupling between the triplet Fe(IV) and the excited triplet porphyrin, and one Fe(IV) d–d transition. Although these transitions are calculated to have zero oscillator strengths, they are not dipole forbidden through symmetry. The normal bands of heme proteins, the Q and B (Soret), are estimated to be within 2000 cm^{-1} of the experimental frequencies. The Q band consists almost purely of transitions from porphyrin $3a_{2u}$ and $1a_{1u}$ to $4e_g$, consistent with the original four-orbital model.[43] The intense Soret Band (B), however, has a substantial amount of mixing with the charge-transfer (CT) excitations $(Cl-Fe-O\ \sigma_2,4e_g)$ and $(3a_{2u}-\sigma_2,\pi_3^*)$. As a result of this mixing, a "split Soret" is calculated, as it was for carbonyl ferrous P450.[44] These two Soret bands are labeled as B and B′. Experimentally, however, the split Soret is not observed. There are two possible causes for the discrepancy. One is that the actual split between B and B′ is two small to be detected and the other is that the intensity of B′ is substantially smaller than B and it becomes a shoulder of B (see Figure 3a).

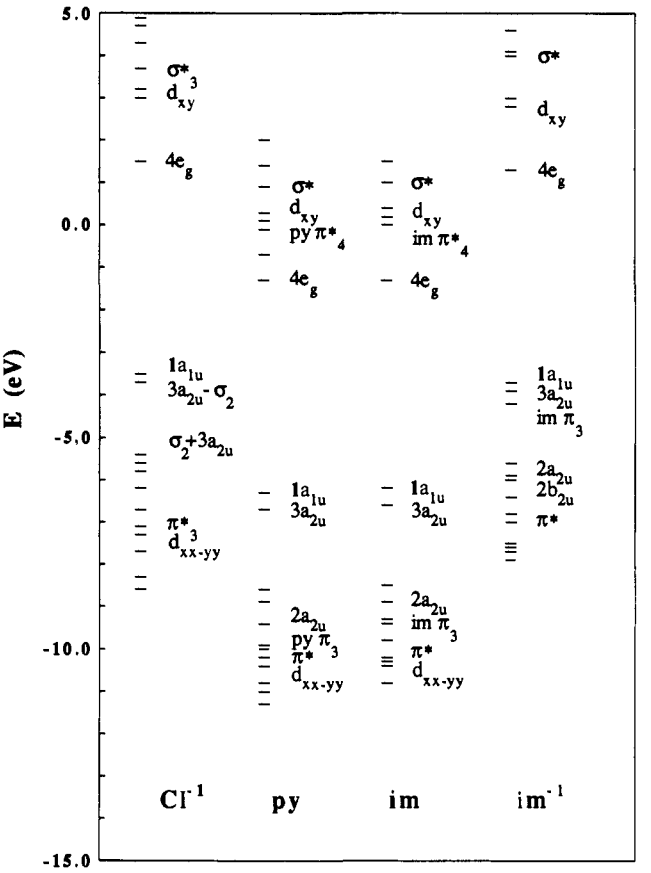

Figure 2. MO energy diagram for model compound II. Only active MOs in the CI-S are included. MOs up to $1a_{1u}$ are doubly occupied. Two electrons occupy the degenerate Fe–O π^* orbitals, short handed as π_3^* for hemin-II and π^* for all other complexes. This occupancy gives the ground state of all compounds $^3A_2$-like symmetry (see text).

The transitions at 17 and 22 kK are assigned as the extra features of the electronic spectrum observed experimentally for

(43) Gouterman, M.; Wagniere, G. H. *J. Mol. Spectrosc.* **1963**, *11*, 108.
(44) Loew, G. H.; Rohmer, M. M. *J. Am. Chem. Soc.* **1980**, *102*, 3655.

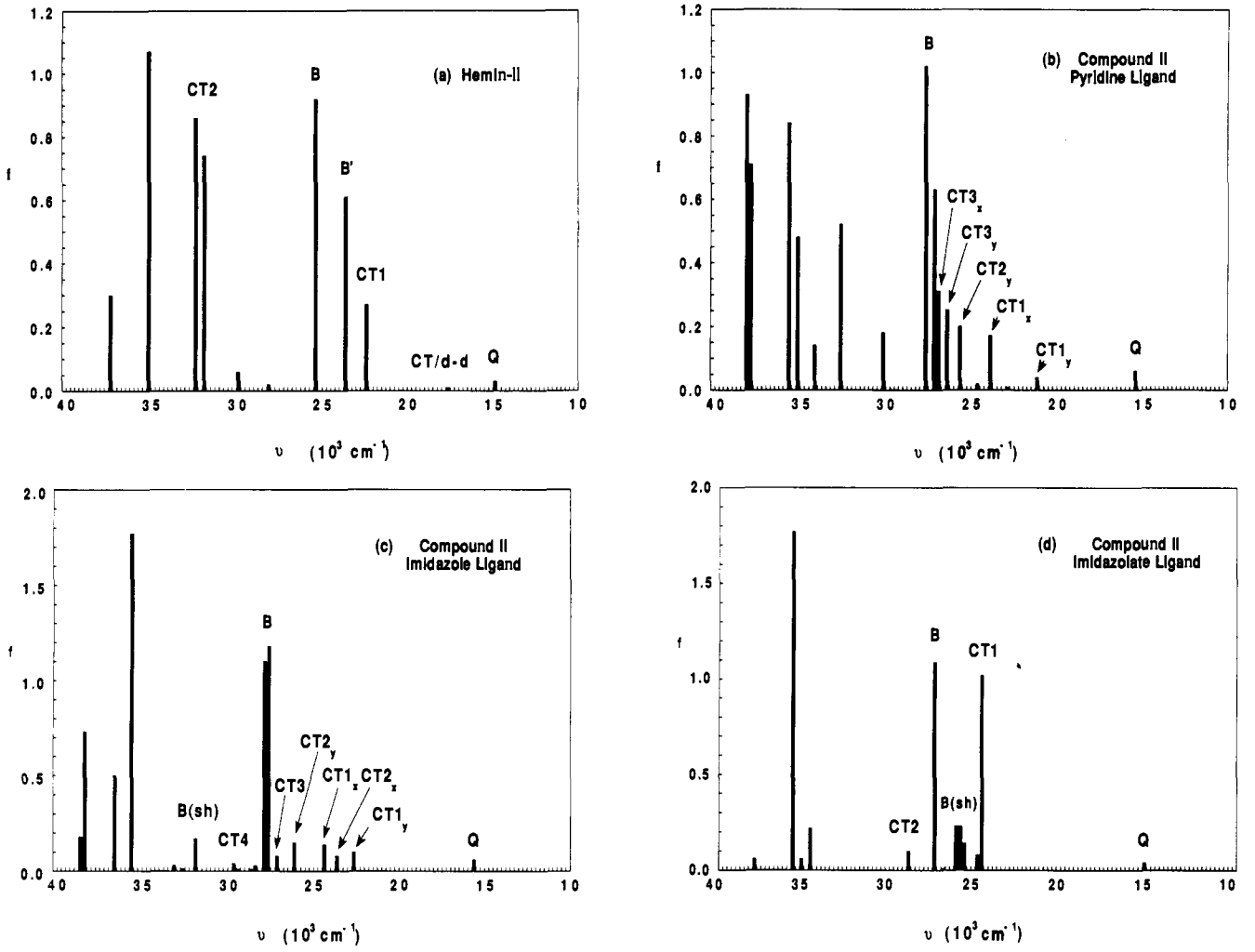

Figure 3. Calculated spectra for the model compound II complexes with the INDO method. Comparisons with experiments and detailed descriptions of the calculated excited states are given in Tables IV–VII. States with energy difference 0.2 kK or smaller are represented with a single line.

the model hemin-II complex. There are three weak transitions near 17 kK, two of which, 5^3E and 7^3E, are the porphyrin Soret-type ($1a_{1u}$,$4e_g$) and ($3a_{2u}$–σ_2,$4e_g$) excitations. The third, 6^3E, is dominated by the (π_3*,d_{xy}) excitation. Since the π_3* orbitals have coefficients on both Fe $3d_\pi$ and O $2p_\pi$, this transition is labeled with Fe(IV) d–d and CT. The absorption intensity calculated for 9^3E (CT2) is moderate. This state has a complex wave function characterized by two dominant configurations. Both configurations are CT in nature. The first is an excitation from σ_2, which is mostly Cl $2p_z$, to $4e_g$, and the second involved a transition from $3a_{2u}$ to π_3*, which is largely on Fe(IV) d_π. A third configuration contributing to this state is the porphyrin ($1a_{1u}$,$4e_g$) transition. The moderate charge-transfer absorption at 31.7 kK was labeled as CT2.

Some z-polarized transitions of $^3A_2$ symmetry are also found for Hemin-II with relatively high frequencies and small oscillator strengths. Three of these states, 5^3A_2, 7^3A_2, and 10^3A_2, result from a mixture of porphyrin ($3e_g$,$4e_g$) and CT excitations. The small oscillator strengths calculated for these transitions are not surprising as they are symmetry forbidden in D_{4h} and gain intensity through the reduction of symmetry caused by the difference between the axial ligands O and Cl. The fourth z-polarized transition, 8^3A_2, is a mixture of three different CT transitions. Since all z-polarized CT transitions are weak, they are likely to be buried in the neighboring strong Soret and CT2 bands. Single-crystal polarized absorption spectra of Hemin-II, however, may verify the presence of these predicted transitions.

II. The Pyridine Compound II Complex. The calculated $^3A_2$ ground-state properties of the model compound II complex with pyridine as the fifth ligand (Table I) show that the electron populations of the Fe and O atoms are significantly reduced, while the spin densities remain essentially unchanged from those results for Hemin-II. Fe(IV) is less positively charged because the N atom of the pyridine ligand is less electron negative than Cl. The negative charge of the porphyrin moiety is only slightly reduced. Since pyridine is neutral, the total charge of the complex is zero. Because of the similar electronic environment for Fe that exists in these two complexes, similar nuclear quadruple splittings and anisotropic hyperfine constants are found.

The energy diagram of the 27 active MOs used in the CI-S calculation are also shown in Figure 2. In addition to the most important porphyrin π and Fe–O orbitals, some pyridine π and π* orbitals (denoted as py π and py π*) are included in this active orbital set. In the subsequent tables and text, the Fe–O d_π–p_π and d_{z^2}–p_z orbitals are simply noted as π and σ. Table V lists the calculated transitions for this complex. Since the pyridine complex has only C_{2v} symmetry, the excitation energies and oscillator strengths calculated for $^3B_1$ and $^3B_2$ excited states do not match exactly. As a result, absorptions with unequal x and y polarization are predicted for the complex. This difference in the degree of x and y polarization, however, is small, indicating a minimum perturbation of the pyridine ligand to the spectra. A plot of the calculated spectrum is shown in Figure 3b.

The triptriplet and d–d transitions are again found to be low-lying in energy. The Q bands are pure porphyrin excitations and the calculated frequencies of the x and y components are 15.2 and 15.4 kK. The B bands are composed of a cluster of excited states near 27 kK. These states all possess substantial CT character, with excitations from $1a_{1u}$ and $3a_{2u}$ to π* and py π_4* being important. There is also some mixing with the pyridine transition (py π_3,py π_4*). Collectively these transitions form a

Table V. INDO/S CI-S Calculated Excited States of Model Compound II with Pyridine Ligand

theory[a]						experiment[c]	
state	configuration contribution[b]	ΔE, kK	$f \times 10^3$	polarization	label	ΔE, kK	$\epsilon \times 10^{-3}$, mM^{-1} cm^{-1}
1^3B_2	($1a_{1u}$,$4e_g$) 0.75, ($3a_{2u}$,$4e_g$) 0.17	9.4	0		$triplet_x$		
1^3B_1	($1a_{1u}$,$4e_g$) 0.77, ($3a_{2u}$,$4e_g$) 0.15	9.4	0		$triplet_y$		
2^3B_2	($d_{x^2-y^2}$,π^*) 0.96	10.7	0		$(d-d)_x$		
2^3B_1	($d_{x^2-y^2}$,π^*) 0.96	10.8	0		$(d-d)_y$		
3^3B_2	($3a_{2u}$,$4e_g$) 0.76, ($1a_{1u}$,$4e_g$) 0.19	12.3	0		$triplet_x$		
3^3B_1	($3a_{2u}$,$4e_g$) 0.79, ($1a_{1u}$,$4e_g$) 0.16	12.5	0		$triplet_y$		
4^3B_2	($1a_{1u}$,$4e_g$) 0.54, ($3a_{2u}$,$4e_g$) 0.40	15.2	25	x	Q_x	17.0	0.08
4^3B_1	($1a_{1u}$,$4e_g$) 0.55, ($3a_{2u}$,$4e_g$) 0.40	15.4	31	y	Q_y		
6^3B_2	(π^*,d_{xy}) 0.89	18.1	3	x	$(d-d)_x$		
6^3B_1	(π^*,d_{xy}) 0.88	18.3	4	y	$(d-d)_y$		
7^3B_1	($3a_{2u}$,$4e_g$) 0.67, ($1a_{1u}$,$4e_g$) 0.18	19.1	3	y			
7^3B_2	($3a_{2u}$,$4e_g$) 0.74, ($1a_{1u}$,$4e_g$) 0.17	19.2	1	x			
8^3B_2	($1a_{1u}$,py π_4^*) 0.61, ($1a_{1u}$,π^*) 0.28	20.8	6	x			
8^3B_1	($3a_{2u}$,π^*) 0.36, ($3a_{2u}$,py π_4^*) 0.35	21.1	37	y	$CT1_y$	17.9	0.16
9^3B_2	($1a_{1u}$,py π_4^*) 0.95	22.8	10	x			
10^3B_2	($3a_{2u}$,π^*) 0.59, ($2a_{2u}$,π^*) 0.10, ($3a_{2u}$,$4e_g$) 0.08	23.7	169	x	$CT1_x$	18.4	0.14
9^3B_1	($3a_{2u}$,py π_4^*) 0.95	24.4	13	y			
6^3A_2	(py π_3,py π_4^*) 0.63	24.6	1	z			
7^3A_2	($3e_g$,$4e_g$) 0.32, ($3e_g$,π^*) 0.21	24.6	10	z			
10^3B_1	(π^*,σ^*) 0.85	25.0	5	y			
11^3B_2	(π^*,σ^*) 0.85	25.1	2	x			
11^3B_1	($1a_{1u}$,π^*) 0.71	25.5	196	y	$CT2_y$		
12^3B_1	($3a_{2u}$,py π_4^*) 0.38, ($1a_{1u}$,π^*) 0.16, ($1a_{1u}$,$4e_g$) 0.09	26.3	250	y	$CT3_y$		
12^3B_2	(py π_3,py π_4^*) 0.16, ($1a_{1u}$,π^*) 0.16, ($1a_{1u}$,π^*) 0.13	26.7	311	x	$CT3_x$		
13^3B_1	($2a_{2u}-\sigma$,$4e_g$) 0.34, ($2b_{2u}$,$4e_g$) 0.25, ($3e_g-\pi$,$2b_{1u}$) 0.13	26.9	219	y	B_y		
13^3B_2	(py π_3,py π_4^*) 0.28, ($2a_{2u}-\sigma$,$4e_g$) 0.19, ($2b_{2u}$,$4e_g$) 0.14	27.0	51	x			
14^3B_2	(py π_3,py π_4^*) 0.32, ($1a_{1u}$,π^*) 0.11, ($3a_{2u}$,$4e_g$) 0.10	27.1	274	x	B_x		
15^3B_2	($1a_{1u}$,py π_4^*) 0.21, ($1a_{1u}$,π^*) 0.17, ($3a_{2u}$,$4e_g$) 0.14	27.4	444	x	B_x		
14^3B_1	($3a_{2u}$,$4e_g$) 0.20, ($3a_{2u}$,py π_4^*) 0.18, ($3a_{2u}$,π^*) 0.15	27.6	586	y	B_y	23.8	1.90
9^3A_2	($1a_{1u}$,py π_5^*) 0.99	28.0	2	z			
12^3A_2	($3a_{2u}$,σ^*) 0.65	29.6	17	z			
15^3B_1	($3e_g-\pi$,σ^*) 0.32, (π_y+3e_g-py π_2,σ^*) 0.25, ($3a_{2u}$,$4e_g$) 0.09	30.8	169	y			
18^3B_1	($3e_g-\pi$,d_{xy}) 0.45, (π_x+3e_g,d_{xy}) 0.17, ($2b_{2u}$,$4e_g$) 0.11	32.7	523	y			
21^3B_1	($2b_{2u}$,$4e_g$) 0.16, ($2a_{2u}-\sigma$,$4e_g$) 0.15, ($\sigma+1b_{1u}$,π^*) 0.10	33.9	141	y			
25^3B_2	($2b_{2u}$,$4e_g$) 0.31, ($2a_{2u}-\sigma$,$4e_g$) 0.16, ($1a_{1u}$,$5e_g$) 0.07	35.1	475	x			
24^3B_1	($2b_{2u}$,$4e_g$) 0.38, ($3e_g-\pi$,d_{xy}) 0.13, ($2a_{2u}-\sigma$,$4e_g$) 0.11	35.4	840	y			
25^3B_1	($2a_{2u}-\sigma$,$4e_g$) 0.57, ($2b_{2u}$,$4e_g$) 0.29	37.8	714	y			
28^3B_2	($2a_{2u}-\sigma$,$4e_g$) 0.36, (py π_3,py π_4^*) 0.22, ($2b_{2u}$,$4e_g$) 0.14	38.1	931	x			

[a] E(SCF) = −230.280 832 au. CI-S includes 27 MOs (63–89) of the ground-state $^3A_2$ calculated with ROHF-SCF. [b] See footnote *b* of Table IV. [c] Reference 17.

strong absorption observed as the Soret near 23.8 kK.

CT transitions were found at 21.1 and 23.7 kK (CT1) and at frequencies near the Soret bands (CT2). The two components of CT1 are assigned as the two observed extra peaks at 17.9 and 18.4 kK. The dominant configuration for both of these two states is CT from the porphyrin to Fe–O ($3a_{2u}$,π^*). Substantial mixing in the CT of transitions from the porphyrin to pyridine ($3a_{2u}$,py π_4^*), however, is found for $CT1_y$. As a result, $CT1_y$ is stabilized by 1.4 kK relative to $CT1_x$. These two absorptions have moderate oscillator strengths, consistent with the experimental intensities. The CT2 and CT3 transitions are so close to B in energies that they are unlikely to be observed. Several weak transitions between 18 and 20 kK were calculated. These are the triptriplet and Fe(IV) d–d excitations. There are also a few weak CT transitions found between 24 and 25 kK.

III. The Imidazole and Imidazolate Model Peroxidase Compound II Complexes. Since the $H_{\delta 1}$ atom (Figure 1) is hydrogen-bonded to an amino acid in peroxidases and can easily dissociate in the protein environment, we have included in the study of the imidazole model peroxidase compound II complexes the effect of deprotonation on the CT transitions. The geometries for the imidazole and imidazolate ligands were optimized with the AM1 method.[41] C_s symmetry was assumed for both imidazole and imidazolate complexes. The ground-state triplet is $^3A''$, whose properties calculated with the ROHF-SCF wave function for both complexes show good agreement with experimental results for HRP and CCP (Table I). The spin density on the O atom was calculated to be 0.20 for O $2p_x$ and $2p_y$, in comparison with the experimentally inferred value of 0.25.[21] The nuclear quadruple splitting of 1.52 mm/s calculated for the neutral imidazole complex and 1.43 for the imidazolate anion complex are close to the value of 1.46 determined experimentally.[18] Thus, these ground-state properties are insensitive to the deprotonation of imidazole.

To explore the effect of imidazole deprotonation on the absorption spectra of model compound II was the next logical step of this study. Similar CI calculations were performed separately for the imidazole and the imidazolate complexes. The active MOs for CI-S shown in Figure 2 include some imidazole π orbitals, whose energies are greatly affected by deprotonation. With the building up of a negative charge on imidazole as a result of deprotonation, the imidazole π orbital energies are increased relative to the porphyrin orbitals. This relative shift of orbital energies could change the qualitative nature of CT transitions involving imidazole. The $N_{\delta 1}$ sp^2 lone pair orbital of the imidazolate ligand was also included in the CI. As shown in the following discussions, excitations from this MO do not make significant contributions to the spectrum.

Table VI and Figure 3c show the calculated transitions with the neutral imidazole ligand. CT transitions (CT1 and CT2) with moderate oscillator strengths were found at 22.7, 23.5, 24.3, and 25.9 kK. They originate from ($3a_{2u}$,π^*) for CT1 and ($1a_{1u}$,π^*) for CT2. One component of each ($CT1_y$ and $CT2_x$) is mixed with excitations from porphyrin to the imidazole π_4^* orbital. As a result of this mixing, the energies of these two states are lower than the other components ($CT1_x$ and $CT2_y$). The two components of CT1 were calculated to have larger oscillator strengths and are assigned to the observed extra peaks for CCP at 17.9 and 18.9 kK.

The CT transitions with excitations from porphyrin π to ligand π^* orbital were found to be higher in energy. Two states, $19^3A''$ (CT3) and $25^3A'$ (CT4), are predominantly of transitions ($1a_{1u}$,im

Table VI. INDO/S CI-S Calculated Excited States of Model Compound II with Imidazole Ligand

theory[a]						experiment[c]	
state	configuration contribution[b]	ΔE, kK	$f \times 10^3$	polarization	label	ΔE, kK	$\epsilon \times 10^3$, mM^{-1}, cm^{-1}
$1^3A'$	$(1a_{1u},4e_g)$ 0.80, $(3a_{2u},4e_g)$ 0.13	9.9	0		$triptriplet_y$		
$2^3A''$	$(1a_{1u},4e_g)$ 0.81, $(3a_{2u},4e_g)$ 0.13	10.1	0		$triptriplet_x$		
$2^3A'$	$(d_{x^2-y^2},\pi^*)$ 0.96	10.8	0		$(d-d)_y$		
$3^3A''$	$(d_{x^2-y^2},\pi^*)$ 0.96	10.9	0		$(d-d)_x$		
$3^3A'$	$(3a_{2u},4e_g)$ 0.80, $(1a_{1u},4e_g)$ 0.15	12.5	0		$triptriplet_y$		
$4^3A''$	$(3a_{2u},4e_g)$ 0.82, $(1a_{1u},4e_g)$ 0.14	12.7	0		$triptriplet_x$		
$4^3A'$	$(1a_{1u},4e_g)$ 0.54, $(3a_{2u},4e_g)$ 0.42	15.5	32	y	Q_y	15.5	0.04
$5^3A''$	$(1a_{1u},4e_g)$ 0.55, $(3a_{2u},4e_g)$ 0.41	15.7	30	x	Q_x		
$8^3A'$	(π^*,d_{xy}) 0.89	18.3	3	y	$(d-d)_y$		
$8^3A''$	(π^*,d_{xy}) 0.89	18.4	2	x	$(d-d)_x$		
$9^3A'$	$(3a_{2u},4e_g)$ 0.76, $(1a_{1u},4e_g)$ 0.16	19.3	2	y			
$9^3A''$	$(3a_{2u},4e_g)$ 0.80, $(1a_{1u},4e_g)$ 0.15	19.5	1	x			
$14^3A'$	$(3a_{2u},\pi^*)$ 0.56, $(3a_{2u},im\ \pi_4^*)$ 0.14	22.7	97	y	$CT1_y$	17.9	0.13
$13^3A''$	$(1a_{1u},\pi^*)$ 0.49, $(1a_{1u},im\ \pi_4^*)$ 0.27	23.5	83	x	$CT2_x$		
$14^3A''$	$(3a_{2u},\pi^*)$ 0.57, $(1a_{1u},4e_g)$ 0.08	24.3	143	x	$CT1_x$	18.9	0.12
$15^3A''$	(π^*,σ^*) 0.86	25.4	7	x	$(d-d)_x$		
$16^3A'$	(π^*,σ^*) 0.88	25.5	3	y	$(d-d)_y$		
$16^3A''$	$(3e_g-\pi,4e_g)$ 0.62	25.7	3	z			
$17^3A'$	$(1a_{1u},\pi^*)$ 0.84	25.9	144	y	$CT2_y$		
$17^3A''$	$(3e_g-\pi,4e_g)$ 0.50, $(3e_g-\pi,\pi^*)$ 0.12	26.0	12	z			
$18^3A''$	$(im\ \pi_3-2b_{2u},im\ \pi_5^*)$ 0.43, $(im\ \pi_3-2b_{2u},im\ \pi_4^*)$ 0.25	26.3	1	x			
$19^3A''$	$(1a_{1u},im\ \pi_4^*)$ 0.87	27.0	78	x	CT3		
$19^3A'$	$(3a_{2u},4e_g)$ 0.30, $(1a_{1u},4e_g)$ 0.26, $(3a_{2u},im\ \pi_4^*)$ 0.10	27.4	1178	y	B_y	23.8	1.60
$20^3A''$	$(3a_{2u},4e_g)$ 0.32, $(1a_{1u},4e_g)$ 0.21, $(1a_{1u},im\ \pi_4^*)$ 0.10	27.6	1098	x	B_x		
$21^3A''$	$(im\ \pi_3-2b_{2u},im\ \pi_4^*)$ 0.47, $(im\ \pi_3-2b_{2u},im\ \pi_5^*)$ 0.26	27.7	4	x			
$20^3A'$	$(3e_g-\pi,4e_g)$ 0.65, $(1a_{1u},2b_{1u})$ 0.14	28.1	4	y			
$21^3A'$	$(3a_{2u},4e_g)$ 0.79	28.2	25	y			
$23^3A'$	$(1a_{1u},2b_{1u})$ 0.38, $(2a_{2u}-\sigma,4e_g)$ 0.10, $(2b_{2u}-im\ \pi_3,4e_g)$ 0.10	28.4	10	y			
$22^3A''$	$(2a_{2u}-\sigma,4e_g)$ 0.40, $(2b_{2u}-im\ \pi_3,4e_g)$ 0.33	28.4	1	x			
$23^3A''$	$(3e_g-\pi,4e_g)$ 0.41, $(3a_{2u},\sigma^*)$ 0.12, $(3e_g-\pi,\pi^*)$ 0.08	28.7	1	z			
$24^3A''$	$(1a_{1u},im\ \pi_4^*)$ 0.54, $(1a_{1u},\pi^*)$ 0.23	29.3	10	x			
$25^3A''$	$(3e_g-\pi,4e_g)$ 0.49, $(1a_{1u},im\ \pi_4^*)$ 0.12, $(1a_{1u},3b_{2u})$ 0.09	29.4	1	x			
$25^3A'$	$(3a_{2u},im\ \pi_4^*)$ 0.72	29.6	37	y	CT4		
$31^3A''$	$(3e_g-\pi,\sigma^*)$ 0.45, (π_x+3e_g,σ^*) 0.38	31.9	174	x	B(sh)	29.4	0.26
$32^3A'$	$(3e_g-\pi,d_{xy})$ 0.47, (π_x+3e_g,d_{xy}) 0.20	32.5	105	y			
$33^3A'$	$(2a_{2u}-\sigma,4e_g)$ 0.33, $(2b_{2u}-im\ \pi_3,4e_g)$ 0.32	33.0	31	y			
$44^3A''$	$(3e_g-\pi,d_{xy})$ 0.28, $(2b_{2u}-im\ \pi_3,4e_g)$ 0.18, $(2a_{2u}-\sigma,4e_g)$ 0.15	35.5	770	x			
$40^3A'$	$(1a_{1u},\sigma^*)$ 0.16, $(2b_{2u}-im\ \pi_3,4e_g)$ 0.16, $(3e_g-\pi,\sigma^*)$ 0.14	35.5	920	y		36.0	0.72
$41^3A'$	$(1a_{1u},\sigma^*)$ 0.75	35.6	186	y			
$47^3A''$	$(3e_g-\pi,d_{xy})$ 0.49, $(\pi_y+3e_g-im\ \pi_2,d_{xy})$ 0.23	36.4	312	x			
$44^3A'$	$(3e_g-\pi,\sigma^*)$ 0.38, $(\pi_y+3e_g-im\ \pi_2\sigma^*)$ 0.23, $(2b_{2u}-im\ \pi_3,4e_g)$ 0.12	36.5	183	y			
$49^3A'$	$(2a_{2u}-\sigma,4e_g)$ 0.42, $(2b_{2u}-im\ \pi_3,4e_g)$ 0.22	38.2	503	y			
$54^3A''$	$(2a_{2u}-\sigma,4e_g)$ 0.32, $(2b_{2u}-im\ \pi_3,4e_g)$ 0.20, $(3a_{2u},\sigma^*)$ 0.19	38.4	226	x			
$45^3A''$	$(1a_{1u},3b_{2u})$ 0.17, $(\pi_y+3e_g-im\ \pi_2,4e_g)$ 0.16, $(2a_{2u}-\sigma,4e_g)$ 0.11	38.6	101	x			
$50^3A'$	$(\pi,4e_g)$ 0.46, $(im\ \pi_3,4e_g)$ 0.11, $(2a_{2u}-\sigma,4e_g)$ 0.09	38.6	75	y			

[a] $E(SCF) = -227.315\,386$ au. CI-S includes 23 MOs (63–85) of the ground-state $^3A''$ calculated with ROHF-SCF. [b] See footnote *b* of Table IV. [c] Reference 28.

π_4^*) and $(3a_{2u},im\ \pi_4^*)$. Their energies are estimated to be 27.0 and 29.6 kK, respectively. CT3 is very close to the calculated Soret band and would be buried under it. CT4 has a small oscillator strength and is near the shoulder of the Soret experimentally observed at 24.9 kK. There are a series of strong multiconfigurational transitions near 35–36 kK, and they are assigned to the observed absorptions at 36 kK.

The calculated spectrum of the imidazolate ligand complex is shown in Table VII and Figure 3d. Similar to the results found for the neutral imidazole complex, CT1 was calculated to be near 24 kK with a dominant configuration $(3a_{2u},\pi^*)$. The oscillator strength, however, is substantially larger than that of the imidazole complex. Another contrast to the neutral ligand is that there is no mixing in porphyrin to Fe(IV) CT transitions of excitation that involve the ligand. As a result, the CT_x and CT_y components are nearly degenerate. The excitation energy of CT2 $(1a_{1u},\pi^*)$ was found to be higher than B. CT transitions from im π_3 to $4e_g$ ($10^3A''$, $16^3A'$, and $12^3A''$, noted as CT3) were found to be rather low in energy, presumably because of the high MO energy of im π_3 (Figure 2). The oscillator strengths for these transitions are however very small.

The clustered states between 26 and 27 kK with significant intensities are assigned to the Soret bands (B) because they all are due to porphyrin (π,π^*) excitations. Since the frequencies of these transitions are very close together, they would appear as a single peak. The strong transition around 35 kK was assigned to an observed absorption at 36.0 kK. In all of the excited states calculated, no significant contribution of the excitations from the $N_{\delta 1}$ lone pair electrons were found.

These results show that the model compound II complex with both the neutral and deprotonated anion form of imidazole as a ligand display extra CT features. The absorption frequencies of these CT, CT1 specifically, are between the Q and the B. The dominant configurations of these states for both complexes are the electron excitation from a porphyrin orbital to the Fe–O π^* orbital. The major difference is that, in the neutral complex, there is substantial mixing of porphyrin to ligand CT configuration $(1a_{1u},im\ \pi_4^*)$ in the wave function. This mixing is a direct result of the relatively low orbital energy for the π_4^* of neutral imidazole (Figure 2). Consequently the degenerate CT transition in the neutral ligand complex is split, with the energy of CT_y being lowered.

Conclusion

Charge-transfer transitions that account for the extra observed features between the Q and B bands were found for all model compound II complexes studied. These CT transitions have calculated oscillator strengths intermediate between those cal-

Table VII. INDO/S CI-S Calculated Excited States of Model Compound II with Imidazolate Ligand

theory[a]						experiment[c]	
state	configuration contribution[b]	ΔE, kK	$f \times 10^3$	polarization	label	ΔE, kK	$\epsilon \times 10^3$, mM^{-1} cm^{-1}
$1^3A'$	$(1a_{1u},4e_g)$ 0.68, $(3a_{2u},4e_g)$ 0.24	9.7	0		$triptriplet_y$		
$2^3A''$	$(1a_{1u},4e_g)$ 0.68, $(3a_{2u},4e_g)$ 0.25	9.9	0		$triptriplet_x$		
$2^3A'$	$(d_{x^2-y^2},\pi^*)$ 0.96	10.4	0		$(d-d)_y$		
$3^3A''$	$(d_{x^2-y^2},\pi^*)$ 0.96	10.6	0		$(d-d)_x$		
$3^3A'$	$(3a_{2u},4e_g)$ 0.70, $(1a_{1u},4e_g)$ 0.27	11.8	0		$triptriplet_y$		
$4^3A''$	$(3a_{2u},4e_g)$ 0.69, $(1a_{1u},4e_g)$ 0.27	12.0	0		$triptriplet_x$		
$4^3A'$	$(1a_{1u},4e_g)$ 0.51, $(3a_{2u},4e_g)$ 0.45	15.1	20	y	Q_y	15.5	0.04
$5^3A''$	$(1a_{1u},4e_g)$ 0.51, $(3a_{2u},4e_g)$ 0.45	15.3	20	x	Q_x		
$7^3A''$	(π^*,d_{xy}) 0.90	17.7	2	x	$(d-d)_x$		
$8^3A'$	(π^*,d_{xy}) 0.89	17.9	3	y	$(d-d)_y$		
$10^3A''$	$(im\ \pi_3,4e_g)$ 0.92	21.5	3	x	$CT3_x$		
$16^3A'$	$(im\ \pi_3,4e_g)$ 0.96	21.7	1	y	$CT3_y$		
$12^3A''$	$(im\ \pi_3,4e_g)$ 0.89	22.0	3	x	$CT3_x$		
$18^3A'$	$(3a_{2u},\pi^*)$ 0.34, $(1a_{1u},4e_g)$ 0.18, $(3a_{2u},4e_g)$ 0.15	24.7	557	y	$CT1_y$	17.9	0.13
$14^3A''$	$(3a_{2u},\pi^*)$ 0.31, $(1a_{1u},4e_g)$ 0.16, $(3a_{2u},4e_g)$ 0.12	24.7	462	x	$CT1_x$		
$15^3A''$	$(3e_g-\pi,4e_g)$ 0.56, $(3e_g-\pi,\pi^*)$ 0.09	25.0	81	z			
$19^3A'$	$(3e_g,4e_g)$ 0.57, $(2b_{2u},2b_{1u})$ 0.11	24.8	9	y			
$17^3A''$	(π^*,σ^*) 0.81	25.9	1	x	$(d-d)_x$		
$20^3A'$	(π^*,σ^*) 0.83	25.4	6	y	$(d-d)_y$		
$21^3A'$	$(2a_{2u},4e_g)$ 0.33, $(2b_{2u},4e_g)$ 0.23, $(3e_g,2b_{1u})$ 0.09	26.1	234	y	$B(sh)_y$		
$18^3A''$	$(2a_{2u},4e_g)$ 0.32, $(2b_{2u},4e_g)$ 0.22, $(3e_g-\pi,2b_{1u})$ 0.11	26.3	231	x	$B(sh)_x$		
$22^3A'$	$(3e_g,4e_g)$ 0.61	27.3	8	y			
$24^3A'$	$(3a_{2u},\pi^*)$ 0.40, $(3a_{2u},4e_g)$ 0.20, $(1a_{1u},4e_g)$ 0.09	27.4	523	y	B_y	23.8	1.60
$19^3A''$	$(3a_{2u},\pi^*)$ 0.38, $(3a_{2u},4e_g)$ 0.21, $(1a_{1u},4e_g)$ 0.10	27.6	566	x	B_x		
$20^3A''$	$(3e_g-\pi,4e_g)$ 0.58, $(\pi+3e_g,4e_g)$ 0.11	27.9	2	xz			
$22^3A''$	$(im\ \pi_3,4e_g)$ 0.62	28.7	2	xz			
$28^3A'$	$(1a_{1u},\pi^*)$ 0.84	28.9	54	y	$CT2_y$	29.4	0.26
$25^3A''$	$(1a_{1u},\pi^*)$ 0.84	29.1	46	x	$CT2_x$		
$44^3A'$	$(3e_g-\pi,d_{xy})$ 0.41, $(\pi+3e_g,d_{xy})$ 0.19, $(3e_g-\pi,\sigma^*)$ 0.12	34.8	221	y			
$43^3A''$	$(3e_g-\pi,\sigma^*)$ 0.23, $(3e_g-\pi,d_{xy})$ 0.18, $(\pi+3e_g,\sigma^*)$ 0.15	35.2	404	x			
$46^3A'$	$(3e_g-\pi,\sigma^*)$ 0.30, $(3e_g-\pi,d_{xy})$ 0.24, $(\pi+3e_g,\sigma^*)$ 0.14	35.2	233	y			
$49^3A'$	$(3e_g-\pi,\sigma^*)$ 0.24, $(2a_{2u},4e_g)$ 0.18, $(\pi+3e_g,\sigma^*)$ 0.12	35.7	1116	y		36.0	0.72
$46^3A''$	$(3e_g-\pi,d_{xy})$ 0.15, $(1a_{1u},5e_g)$ 0.13, $(2a_{2u},4e_g)$ 0.11	35.8	656	x			
$54^3A'$	$(2a_{2u},4e_g)$ 0.31, $(2b_{2u},4e_g)$ 0.19, $(\sigma+2a_{2u},\pi^*)$ 0.16	38.0	341	y			
$53^3A''$	$(2a_{2u},4e_g)$ 0.19, $(\pi+3e_g,4e_g)$ 0.14, $(2b_{2u},4e_g)$ 0.11	38.0	219	x			

[a] E(SCF) = −226.157 155 au. Cl-S includes 25 MOs (61–85) of the ground-state $^3A''$ calculated with ROHF-SCF. [b] See footnote *b* of Table IV. [c] Reference 28.

culated for Q and B. The type of charge transfer is however somewhat different in each complex. In hemin-II, both the oxygen and chloride ligands are involved in CT to the porphyrin. In the pyridine, imidazole, and imidazolate compound II complexes, the charge transfer is predominantly from the porphyrin π to the Fe–O π^* orbital, but with a different extent of mixing of CT from porphyrin to ligand, which occurs significantly in the pyridine and neutral imidazole complexes. The existence of these CT transition states in relatively low excitation energy regions indicates a possible participation of these transitions in the mechanism of the compound II reduction to the enzyme resting state and in the mechanism of electron transfer from cytochrome *c* to CCP. Comparison of the calculated electronic spectra for the protonated and deprotonated species of the imidazole complex with experimental spectra of the protein–compound II, however, did not allow a definitive conclusion to be drawn about the extent of deprotonation of the imidazole. While, as noted, the deprotonation changes the involvement of the ligand in the CT, the observed extra bands are present in both calculations, with only minor variation in intensity and wavelength.

The calculated spectra of the model compound II complexes match the experiments reasonably well in a qualitative sense. Quantitatively, the experimental excitation energies for the CT transitions are generally lower than the theoretical estimates. The overestimate of excitation energies may be associated with an assumed porphine geometry, particularly the Fe–O distance that remains unchanged in the CT transition, an experiment referring to a system in solution, or a limited configuration interaction.

Some general trends are found for the effect of the overall absorption spectra by changing the ligand. First, the Q band is pure porphyrin (π,π^*) excitations and its frequency and oscillator strength remain constant. Second, there are large changes in the Soret bands because they mix with CT transitions that involve the ligand orbitals. It is predicted that Hemin-II has a split Soret. The Soret bands of the imidazolate complex also consist of two sets of distinct excited states though much closer to each other in energy. These findings are consistent with the early studies on P450, in which the split Soret was predicted as a general phenomenon for an Fe–porphyrin complex with an axial ligand that has a lone electron pair. Third, the CT transition from porphyrin to Fe–O π^* is common for all model complexes studied and they lie between the Q and B in excitation energies. There is mixing of this CT state with the ligand excitations. If the ligand is planar and has a low-lying π^* orbital, e.g., pyridine or imidazole, this mixing results in a small splitting of the degeneracy.

Acknowledgment. This work was supported in part through NSF Grant DMB-9096181 (P.D. and G.H.L.) and through a grant from Eastern Kodak Company (M.C.Z.). S.C. is grateful for support from CNPg for his stay at the University of Florida.